The Cytoplasmic Carbonic Anhydrases βCA2 and βCA4 Are Required for Optimal Plant Growth at Low CO_2[1][OPEN]

Robert J. DiMario, Jennifer C. Quebedeaux[2], David J. Longstreth, Maheshi Dassanayake, Monica M. Hartman, and James V. Moroney*

Department of Biological Sciences, Louisiana State University, Baton Rouge, Louisiana 70808

ORCID IDs: 0000-0002-5056-6868 (R.J.D.); 0000-0003-3123-3731 (M.D.); 0000-0001-7289-9826 (M.M.H.); 0000-0002-3652-5293 (J.V.M.).

Carbonic anhydrases (CAs) are zinc metalloenzymes that interconvert CO_2 and HCO_3^-. In plants, both α- and β-type CAs are present. We hypothesize that cytoplasmic βCAs are required to modulate inorganic carbon forms needed in leaf cells for carbon-requiring reactions such as photosynthesis and amino acid biosynthesis. In this report, we present evidence that βCA2 and βCA4 are the two most abundant cytoplasmic CAs in Arabidopsis (*Arabidopsis thaliana*) leaves. Previously, βCA4 was reported to be localized to the plasma membrane, but here, we show that two forms of βCA4 are expressed in a tissue-specific manner and that the two proteins encoded by *βCA4* localize to two different regions of the cell. Comparing transfer DNA knockout lines with wild-type plants, there was no reduction in the growth rates of the single mutants, *βca2* and *βca4*. However, the growth rate of the double mutant, *βca2βca4*, was reduced significantly when grown at 200 μL L^{-1} CO_2. The reduction in growth of the double mutant was not linked to a reduction in photosynthetic rate. The amino acid content of leaves from the double mutant showed marked reduction in aspartate when compared with the wild type and the single mutants. This suggests the cytoplasmic CAs play an important but not previously appreciated role in amino acid biosynthesis.

Carbonic anhydrases (CAs) are zinc metalloenzymes that catalyze the interconversion of CO_2 and HCO_3^-. Flowering plants possess members of the αCA, βCA, and γCA families. While all three CA families contain zinc, they clearly have evolved independently (Hewett-Emmett and Tashian, 1996). Most αCAs are monomeric, although there are notable exceptions (Whittington et al., 2001; Hilvo et al., 2008; Suzuki et al., 2010, 2011; Cuesta-Seijo et al., 2011). The αCA active site contains a single zinc molecule coordinated by three His residues and a water molecule (Liljas et al., 1972). βCAs also contain a zinc active site, although the coordinating molecules are two Cys residues, a His, and a water molecule (Bracey et al., 1994). The active unit of the βCA is a dimer where the active site is located at the interface of the two monomers (Kimber and Pai, 2000). In contrast, γCAs are trimers that have their active site zinc ion situated at the interface of two subunits coordinated by His residues from both subunits (Kisker et al., 1996; Iverson et al., 2000).

In Arabidopsis (*Arabidopsis thaliana*), there are three γCA proteins and two γ-like proteins that interact to form an extra structure of complex I of the mitochondrial electron transport chain (Perales et al., 2004; Sunderhaus et al., 2006). Although not active in vitro, γCA has been shown to bind inorganic carbon (Martin et al., 2009), affect complex I levels, plant growth, and gas-exchange rates when deleted (Perales et al., 2004; Soto et al., 2015), and cause plant sterility when ectopically overexpressed (Villarreal et al., 2009). Arabidopsis has eight αCA genes, but only αCA1, αCA2, and αCA3 appear to be expressed in leaf tissue. αCA1 has been reported to be localized to the chloroplast in leaf tissue (Villarejo et al., 2005; Burén et al., 2011). The expression of αCA2 and αCA3 is quite low but higher than that of αCA4 to αCA8. The physiological role of the αCAs is unknown.

Arabidopsis has six βCA genes (Moroney et al., 2001), and other plants with sequenced genomes have a similar number of βCA genes (Grigoriev et al., 2012; Kawahara et al., 2013). CAs are highly expressed and can account for up to 1% of the soluble protein in a leaf (Tobin, 1970), with the βCAs being the most highly expressed CA genes in leaves (Fett and Coleman, 1994; Schmid et al., 2005; Fabre et al., 2007; Winter et al., 2007; Hu et al., 2010). The six βCA isoforms are found in a number of subcellular locations. βCA1 and βCA5 have been localized to the chloroplast (Fabre et al., 2007; Hu et al., 2015), while βCA2 and βCA3 are found in the

[1] This work was supported by the National Science Foundation (grant no. IOS–1146597 to J.V.M.).

[2] Present address: Carl R. Woese Institute for Genome Biology, University of Illinois, 1206 West Gregory Drive, Urbana, IL 61801.

* Address correspondence to btmoro@lsu.edu.

The author responsible for distribution of materials integral to the findings presented in this article in accordance with the policy described in the Instructions for Authors (www.plantphysiol.org) is: James V. Moroney (btmoro@lsu.edu).

J.V.M. developed the original research plans; J.V.M., D.J.L., and M.D. supervised the experiments; R.J.D., J.C.Q., and M.M.H. performed the experiments; J.V.M., D.J.L., M.D., and R.J.D. designed the experiments and analyzed results; J.V.M., D.J.L., and R.J.D. wrote the article with contributions from all authors.

[OPEN] Articles can be viewed without a subscription.

www.plantphysiol.org/cgi/doi/10.1104/pp.15.01990

cytosol (Fabre et al., 2007). The two other βCAs, βCA4 and βCA6, have been reported to be localized to the plasma membrane (Fabre et al., 2007; Hu et al., 2010, 2015) and the mitochondria (Fabre et al., 2007; Jiang et al., 2014), respectively.

The abundance of CAs in plant leaves as well as their various subcellular locations suggest that CAs may play multiple roles in plant metabolism, notably fatty acid synthesis, amino acid biosynthesis, and photosynthesis (Hatch and Burnell, 1990; Badger and Price, 1994; Fett and Coleman, 1994; Raven and Newman, 1994; Hoang and Chapman, 2002). Clearly, any metabolic reaction that produces or consumes CO_2 or HCO_3^- has the potential to be affected by CA activity. In *Gossypium hirsutum*, it has been shown that CAs are involved in lipid biosynthesis, as the CA-catalyzed formation of HCO_3^- in the chloroplast can be used by plastidal acetyl CoA carboxylase in the first step of fatty acid biosynthesis. Using the CA inhibitor ethoxyzolamide in cotton embryos decreased radiolabeled ^{14}C incorporation into total lipids (Hoang and Chapman, 2002). Also, tobacco (*Nicotiana tabacum*) cell suspensions incubated with ethoxyzolamide and tobacco CA antisense lines show lower levels of ^{14}C in total lipids (Hoang and Chapman, 2002).

CA activity may play an important role in C_4 photosynthesis, as the majority of carbon fixed by phospho*enol*pyruvate carboxylase (PEPC) that moves through the C_4 cycle initially passes through a CA-catalyzed reaction (Hatch and Burnell, 1990; Badger and Price, 1994). CA antisense constructs, which reduce the activity of cytosolic CA in *Flaveria bidentis* mesophyll cells by at least 70%, lead to diminished rates of photosynthesis, although CA levels must be severely reduced in order to see effects on photosynthesis rates, due to the high enzymatic activity of CA (von Caemmerer et al., 2004). In maize (*Zea mays*), insertional mutants of the *ca1* and *ca2* genes decreased plant growth but led to no significant changes in photosynthesis rates, suggesting possible anapleurotic roles for CA (Studer et al., 2014).

CAs can act as CO_2 sensors in stomates (Hu et al., 2010, 2015) by providing HCO_3^- for the protein kinase OST1, which controls S-type anion channels involved in CO_2-dependent stomatal closing (Xue et al., 2011). Arabidopsis transfer DNA (T-DNA) plants lacking multiple CAs have reduced stomatal response to changing CO_2 concentrations, an overall higher stomatal conductance, and higher stomatal density when compared with wild-type plants (Hu et al., 2010, 2015; Engineer et al., 2014).

The roles of CAs in C_3 photosynthesis are poorly understood. CAs in the cytosol and chloroplast have been proposed to help facilitate the diffusion of inorganic carbon to the chloroplast; however, recent modeling studies indicate that the effect of CA activity in the cytoplasm might be minimal (Badger and Price, 1994; Terashima et al., 2011; Tholen et al., 2012, 2014). Earlier studies using antisense lines show that reducing chloroplast CA levels below 10% of total CA activity in tobacco did not significantly reduce photosynthesis rates (Majeau et al., 1994; Price et al., 1994; Williams et al., 1996). Other tobacco CA antisense lines have shown reduced water use efficiency and increased stomatal conductance (Majeau et al., 1994; Kim, 1997). All of these studies were conducted before it was known that there were multiple CA genes, so it is still possible that other CA isoforms could compensate for the loss of the targeted CA. Therefore, it is unclear which CAs, if any, contributed to CO_2 conductance or fixation in C_3 plants.

Based on previous reports and our preliminary studies, we hypothesize that there are multiple forms of CA in different cell compartments, and these CAs may have overlapping functions. Here, we report our investigation of the physiological roles of cytoplasmic βCAs. We have found that βCA2 and a previously unknown short form of βCA4, βCA4.2, are the most abundant cytoplasmic CAs in Arabidopsis leaves. Using a transgenic plant missing βCA2, βCA4.1, and βCA4.2, we found that these cytosolic CAs are required for optimal growth under low-CO_2 conditions. We put forth the hypothesis that optimal cytosolic PEPC activity requires CA activity.

RESULTS

βCA2 and βCA4 Are Expressed in Leaves

There are eight *αCA* and six *βCA* genes in Arabidopsis (Moroney et al., 2001; Fabre et al., 2007). EST counts from The Arabidopsis Information Resource (TAIR) show that all of the *βCA*s are well expressed and that *αCA1*, *αCA2*, and *αCA3* are weakly expressed. There are few, if any, ESTs that match *αCA4* through *αCA8* (www.arabidopsis.org). RNA was extracted from roots and leaves of Arabidopsis plants for RNA sequencing (RNAseq) analysis to determine which CAs are significantly expressed in leaf tissue (RNAseq data deposited in the National Center for Biotechnology Information Sequence Read Archive database as BioSample:SAMN03339724). Using leaf RNAseq samples, the normalized count of 100-bp reads that mapped uniquely to a CA gene showed that all of the *βCA* genes are expressed in leaves and that the overall quantitative CA expression pattern agrees with the EST data from TAIR (Table I). When assessing the uniquely mapped reads generated from root RNA samples, βCA4 is the highest expressed CA, whereas analyzing the uniquely mapped reads generated from leaf RNA samples, βCA1 is the most highly expressed CA in leaf tissue (Table I).

The *βCA2* RNAseq data did not match any of the models in TAIR (Fig. 1A). In addition, *βCA4* had two distinct forms of mRNA (Fig. 1B). To further assess these observations, uniquely mapped RNAseq reads from root and leaf samples were viewed on a genome browser aligned to the genomic region containing

Table I. *All six βCAs of Arabidopsis are expressed in roots and shoots*

Each *βCA* gene, gene identifiers, number of ESTs, and RNAseq values are listed. RNAseq values are given in reads per kilobase per million mapped reads averaged from three biological replicates for root and shoot samples.

Gene	Gene Identifier	ESTs[a]	RNAseq Reads (Leaves)	RNAseq Reads (Roots)
βCA1	At3g01500	1,538	109,333	662
βCA2	At5g14740	693	34,488	214
βCA3	At1g23730	51	376	21
βCA4	At1g70410	279	7,781	9,026
βCA5	At4g33580	116	2,262	2,443
βCA6	At1g58180	38	1,419	661
ACTIN1	At2g37620	65	1,471	1,056

[a]CA EST values were extracted from TAIR (http://www.arabidopsis.org).

βCA2 in the Arabidopsis reference genome (TAIR 10). RNAseq reads from both root and leaf samples that mapped to the *βCA2* reference gene show that only a short form of *βCA2* is expressed (Fig. 1A). The observed transcription start site is at the predicted second exon, and the predicted protein is significantly shorter than the TAIR 10 model. The short βCA2, now lacking a chloroplast transit peptide, is predicted to be a cytoplasmic protein, in agreement with the findings of Fabre et al. (2007). Mapping the unique reads generated from root and leaf tissue to the *βCA4* reference gene shows two forms of *βCA4* mRNA (Fig. 1B), consistent with a previous report by Aubry et al. (2014). The longer mRNA form, *βCA4.1*, contains two unique 5′ exons and appears to be expressed mainly in shoot tissues of Arabidopsis, whereas the short mRNA form, *βCA4.2*, contains one unique 5′ exon and is expressed in both roots and shoots (Fig. 1B).

The promoter region of *βCA2* and two upstream regions of *βCA4* were PCR amplified and inserted upstream of the *GUS* gene in the pKGWFS7 (GUS) vector to create the constructs *pβCA2*::*GUS*, *pβCA4.1*::*GUS*, and *pβCA4.2*::*GUS* (Fig. 2, A and B). The promoter region *pβCA4.1*::*GUS* starts within the upstream gene, At1g70420, and ends directly upstream of the ATG start site in the second exon of the *βCA4.1* gene. The promoter region *pβCA4.2*::*GUS* starts after the transcription start site of *βCA4.1* and ends directly upstream of the ATG start site of *βCA4.2*. While these promoters were chosen because they displayed GUS expression, it is possible that other promoter variants could give different expression results. As a positive control, an 805-bp region directly upstream of the *βCA1* ATG start site, similar to the promoter region used by Wang et al. (2014), was inserted into the GUS vector to produce the construct *pβCA1*::*GUS*. Three-week-old Arabidopsis

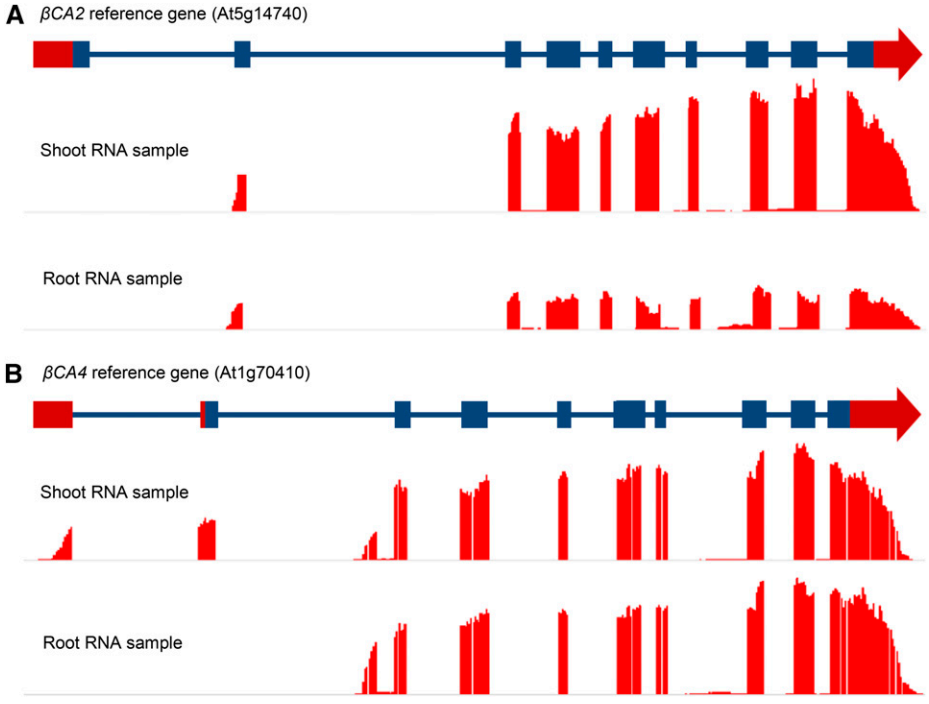

Figure 1. *βCA2* has one mRNA form, while *βCA4* has two mRNA forms. RNAseq reads were aligned to the *βCA2* and *βCA4* gene models in the Arabidopsis reference genome. A, Leaf and root RNA samples yielded one form of *βCA2* mRNA consisting of nine exons, excluding the first exon of the *βCA2* reference gene from TAIR. B, Leaf and root RNA samples yielded two forms of *βCA4* mRNA. The long mRNA form is found primarily in the leaf and contains 10 exons, where the first two exons are unique to the long form. The short mRNA form has nine exons, where the first exon is unique to the short mRNA form and can be found in both the root and shoot RNA samples.

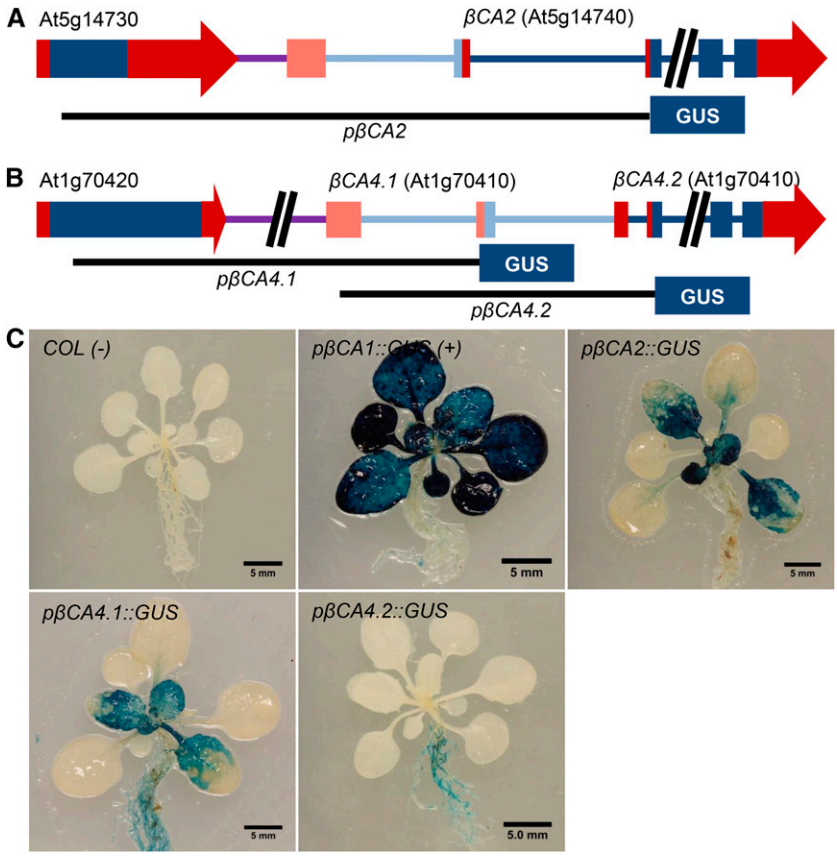

Figure 2. *βCA2* and *βCA4* are both expressed in Arabidopsis leaves. A, Gene fragment of the plus strand of chromosome 5 containing the *βCA2* gene (At5g14740) and the upstream gene (At5g14730). The black line labeled *pβCA2* indicates the genomic region used to control GUS expression. Blue boxes represent exons, red boxes and arrows represent untranslated regions, and blue and purple lines represent introns and intergenic regions, respectively. Light-colored boxes and lines denote alternative versions of the specified gene. B, Fragment of the antisense strand of chromosome 1 containing the *βCA4* gene (At1g70410) and the upstream gene (At1g70420). Black lines labeled *pβCA4.1* and *pβCA4.2* represent the genomic regions used to control GUS expression in the various βCA4::GUS lines. C, Three-week-old Arabidopsis GUS lines grown in ambient CO_2 and constant light showed GUS staining primarily in the leaves of pβCA2::GUS plants, leaves and roots of pβCA4.1::GUS plants, and primarily roots of pβCA4.2::GUS plants.

plants expressing *pβCA1*::*GUS* showed strong GUS expression in the rosette (Fig. 2C). This expression pattern is consistent with βCA1 being the most abundant CA in the leaf and is in agreement with the *βCA1* expression pattern observed by Wang et al. (2014). *pβCA2*::*GUS* and *pβCA4.1*::*GUS* plants also showed GUS expression in their rosettes (Fig. 2B). This confirms the RNAseq data showing that *βCA2*, *βCA4.1*, and *βCA4.2* are expressed in the leaves of Arabidopsis. In addition, the strong GUS staining is consistent with *βCA2* being the second most abundant CA in leaf tissue and both forms of *βCA4* being expressed in leaves.

Subcellular Locations of βCA2, βCA4.1, and βCA4.2

Since the N-terminal sequences of βCA2 and βCA4.2 were different from those predicted by TAIR, the localization of βCA2, βCA4.1, and βCA4.2 was determined. Both coding regions of *βCA4*, *βCA4.1* and *βCA4.2*, were PCR amplified and fused to the N terminus of the *eGFP* gene in the vector, pB7FWG2, to create the constructs βCA4.1-eGFP and βCA4.2-eGFP, powered by the 35S promoter. Also, the coding region of *βCA2* was PCR amplified and fused to the N terminus of the *eGFP* gene to produce the construct βCA2-eGFP, powered by the 35S promoter. When sampling leaves of stable Arabidopsis eGFP lines, the cytoplasmic localization of βCA2-eGFP was confirmed (Fig. 3; Fabre et al., 2007). βCA4.1-eGFP gave a plasma membrane signal as reported by Fabre et al. (2007) and Hu et al. (2010, 2015), but βCA4.2-eGFP was localized to the cytoplasm (Fig. 3). To confirm these results, protoplasts were generated from the stable Arabidopsis eGFP lines. βCA2-eGFP and βCA4.2-eGFP protoplasts gave a cytoplasmic GFP signal, whereas βCA4.1-eGFP protoplasts gave a thin fluorescent signal in a ring surrounding the protoplast, confirming its presence in the plasma membrane (Fig. 4).

βca2 and *βca4* T-DNA Mutants Lack CA Expression

From the localization data, it appears that βCA2 and βCA4.2 are found in the cytoplasm. A third CA, βCA3, also is found in the cytoplasm (Fabre et al., 2007), although its expression is only 1% of the expression of βCA2 and 5% of βCA4 (Table I; Schmid et al., 2005; Winter et al., 2007; Ferreira et al., 2008) and was not considered for this study. To determine the effect of βCA2 and βCA4 on plant growth, T-DNA alleles of each gene, SALK_145785 for the *βca2* line and CS859392 for the *βca4* line, were obtained from TAIR. The SALK_145785 insert is located within the fifth intron of the *βca2* gene, and the CS859392 insert is located in the fourth intron of the *βca4* gene (Fig. 5A). Genomic PCR using *βCA2* and *βCA4* gene-specific primers was generated to show specific T-DNA gene disruptions (Fig. 5,

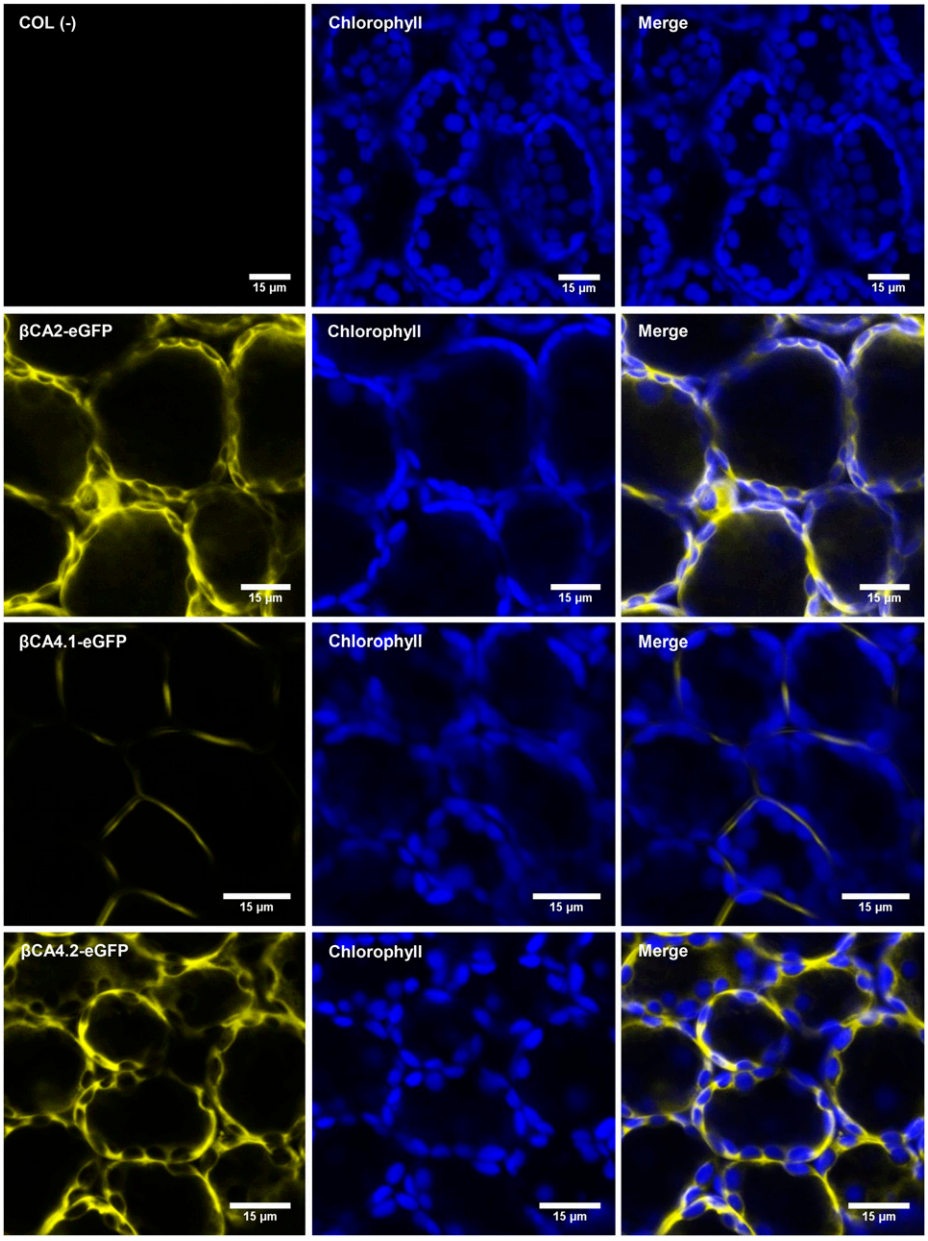

Figure 3. βCA2 and βCA4.2 are located in the cytoplasm, and βCA4.1 is located in the plasma membrane. Sections of intact leaf cells of various eGFP Arabidopsis plants visualized with the confocal microscope show βCA2-eGFP and βCA4.2-eGFP fluorescence in the cytoplasm and βCA4.1-eGFP fluorescence limited to the plasma membrane. Wild-type (COL) leaves were used as a negative control.

A and B). An insert primer was paired with a gene-specific primer to confirm the location of each T-DNA in its respective gene (Fig. 5, A and B). Some mutant lines containing T-DNA insertions within introns are known to show leaky expression of the mutated gene. To confirm that these mutants are T-DNA knockout lines, reverse transcription-PCR was performed using the same genomic primers that span the location of the insert in each gene. The *βCA2* and *βCA4* transcripts are present in the wild type but are absent in their respective mutant lines (Fig. 5C). Transcripts for both genes are absent in the *βca2βca4* line (Fig. 5C).

An antibody raised against spinach (*Spinacia oleracea*) CA (Fawcett et al., 1990) detects protein bands for both βCA1 and βCA2. The βCA1 preprotein consists of 336 amino acids and is directed to the chloroplast (Fabre et al., 2007) by a predicted chloroplast transit peptide of about 103 amino acids (Fawcett et al., 1990; Fett and Coleman, 1994). After cleavage of the chloroplast transit peptide, the mature βCA1 protein has a predicted size of 233 amino acids, yielding a predicted molecular mass of 25.3 kD. βCA2 consists of 259 amino acids with no predicted cleavage site, giving the protein an estimated molecular mass of 28.4 kD. The mature βCA1 and βCA2 proteins are nearly 90% identical, and the antibody detects both proteins (Supplemental Fig. S1). Analysis of wild-type (Columbia [COL]), *βca2*, *βca4*, and *βca2βca4* lines with the spinach CA antibody yielded a 25-kD protein band, indicating the presence of βCA1 in all four samples (Fig. 5D). A second band with

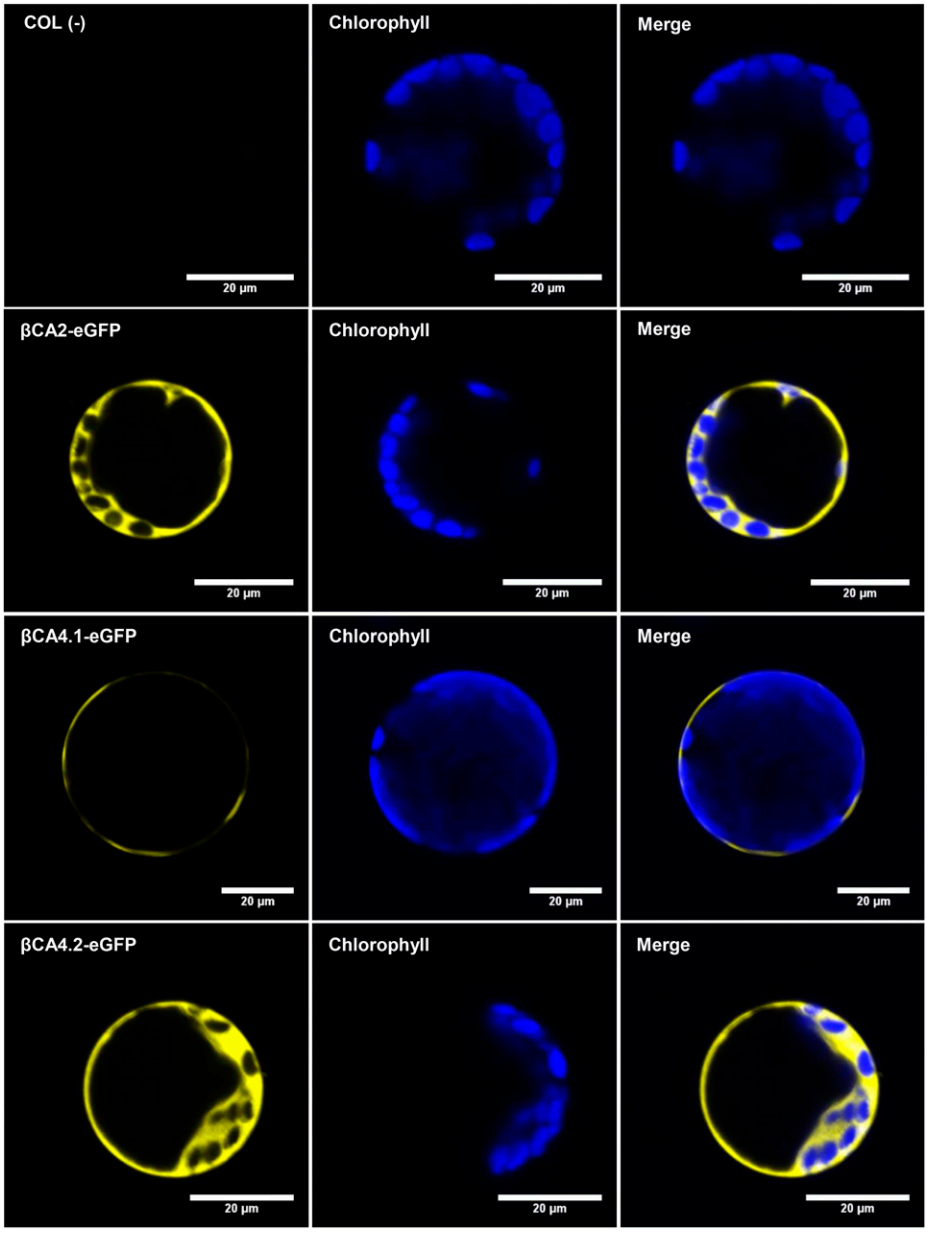

Figure 4. Protoplasts show that βCA2 and βCA4.2 are located in the cytoplasm and βCA4.1 is located in the plasma membrane. Confocal images of leaf cell protoplasts generated from COL, βCA2-eGFP, βCA4.1-eGFP, and βCA4.2-eGFP leaves confirm the presence of βCA2 and βCA4.2 in the cytosol and βCA4.1 in the plasma membrane. Wild-type (COL) leaves were used as a negative control.

a size of 28 kD, which is near the predicted molecular mass of βCA2, can be found in the wild-type (COL) and *βca4* lines but not the *βca2* line or the double mutant, indicating that the βCA2 protein is absent (Fig. 5D).

Growth of the *βca2βca4* Line Is Reduced at Low CO_2 But Not High CO_2

βca2βca4 plants grown for 10 weeks at 200 μL L^{-1} CO_2 and an 8-h daylength were smaller than wild-type (COL), *βca2*, and *βca4* plants (Fig. 6A). Chlorosis also was apparent in the youngest leaves of the *βca2βca4* plants when grown at 200 μL L^{-1} CO_2. In contrast, when grown at 1,000 μL L^{-1} CO_2, rosette areas of *βca2βca4* plants were similar to the rosette areas of wild-type (COL) and the single mutant lines (Fig. 6B). In addition, *βca2βca4* plants were not chlorotic at 1,000 μL L^{-1} CO_2 (Fig. 6B). The weekly average aboveground dry weights and weekly projected rosette areas of the wild-type (COL), *βca2*, and *βca4* lines were similar, but these values were reduced significantly in the *βca2βca4* plants at 200 μL L^{-1} CO_2 (Fig. 7). Dry weight and rosette area of the *βca2βca4* plants grown at low CO_2 were significantly lower than in the other lines by week 2 or 3 of growth (Fig. 7, insets).

Photosynthetic Properties

Photosynthetic properties of individual leaves of 10-week-old wild-type (COL), *βca2*, *βca4*, and *βca2βca4*

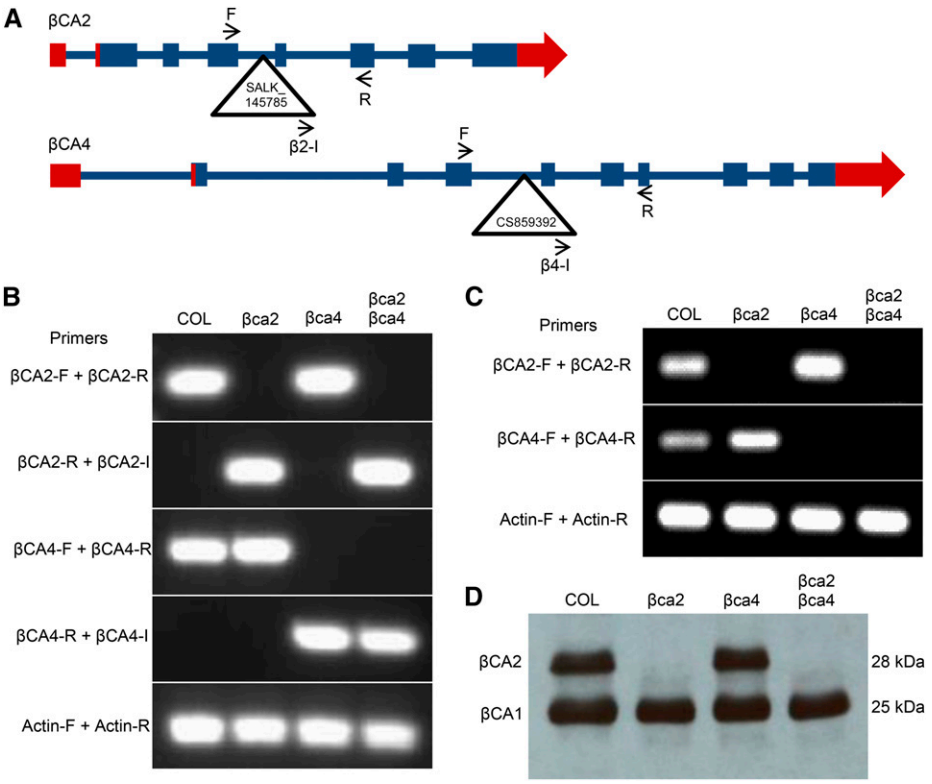

Figure 5. T-DNA insertions in the *βCA2* and *βCA4* genes disrupt RNA synthesis. A, Gene models of *βCA2* and *βCA4*. Blue boxes represent exons, blue lines represent introns, and red boxes represent untranslated regions. Triangles represent locations of each T-DNA insert within its gene. F, Forward primer; I, insert primer; R, reverse primer. Arrows represent the locations and orientations of primers. B, Genomic PCR showing the disruption of the *βCA2* and *βCA4* genes caused by the T-DNA insertions. Actin (At2g37620) was used as a positive control. C, Reverse transcription-PCR showing the absence of the *βCA2* and *βCA4* mRNAs in the various T-DNA lines. Actin (At2g37620) was used as a positive control. D, Western blot showing that the βCA2 protein is missing in the *βca2* and *βca2βca4* plants. Each lane contains 5 μg μL^{-1} of total protein from leaf tissue.

plants grown at 200 μL L^{-1} CO_2 and in an 8-h photoperiod were measured to determine if a reduction in carbon fixation was the cause of the reduced growth in *βca2βca4* under low CO_2. The average CO_2 compensation point of the *βca2βca4* plants was similar to that of the single mutants and wild-type plants (Table II). The rate of CO_2 assimilation in the *βca2βca4* plants was similar to that of the single mutants and wild-type plants when measured at 200, 400, and 1,000 μL L^{-1} CO_2 (Table II).

Free Amino Acid Pools in the *βca2βca4* Mutant

PEPC in the cytoplasm uses HCO_3^- to generate 50% of the Asp in leaf cells of tobacco (Melzer and O'Leary, 1987). Leaf samples from wild-type, *βca2*, *βca4*, and *βca2βca4* plants grown in 200 μL L^{-1} CO_2 were analyzed for amino acid content to determine if Asp levels as well as other amino acid levels are altered in the double mutant. The amino acid levels of wild-type plants are comparable to levels in the single mutants *βca2* and *βca4* (Fig. 8; Supplemental Table S1). In leaf samples of the double mutant, the Asp concentration is only 87 ± 28 μg g^{-1} leaf tissue, well below the levels of wild-type and single mutant plants (Fig. 8; Supplemental Table S1). Interestingly, Glu and Gln levels also are lower in the double mutant, whereas Gly and Ser levels are higher in the double mutant (Fig. 8; Supplemental Table S1).

Complementation Restores Growth of the *βca2βca4* Mutant

To confirm that T-DNA insertions in the *βCA2* and *βCA4* genes are responsible for the reduced growth of the *βca2βca4* line, complementation lines expressing the wild-type *βCA2* coding region powered by a 2× 35S promoter were generated. Reestablishing the wild-type

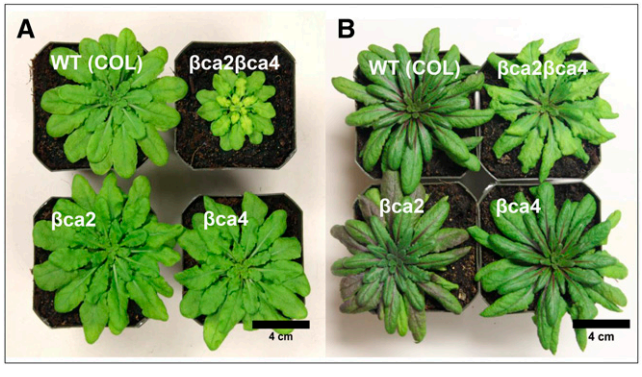

Figure 6. Growth is reduced in the *βca2βca4* line when grown in low CO_2, whereas a high-CO_2 environment restores normal growth in the *βca2βca4* line. Images show 10-week-old plants grown in low (200 μL L^{-1}) CO_2 (A) and high (1,000 μL L^{-1}) CO_2 (B) at a light intensity of 120 μmol photons m^{-2} s^{-1}. All plants were grown under an 8-h-light (22°C)/16-h-dark (18°C) regime. WT, Wild type.

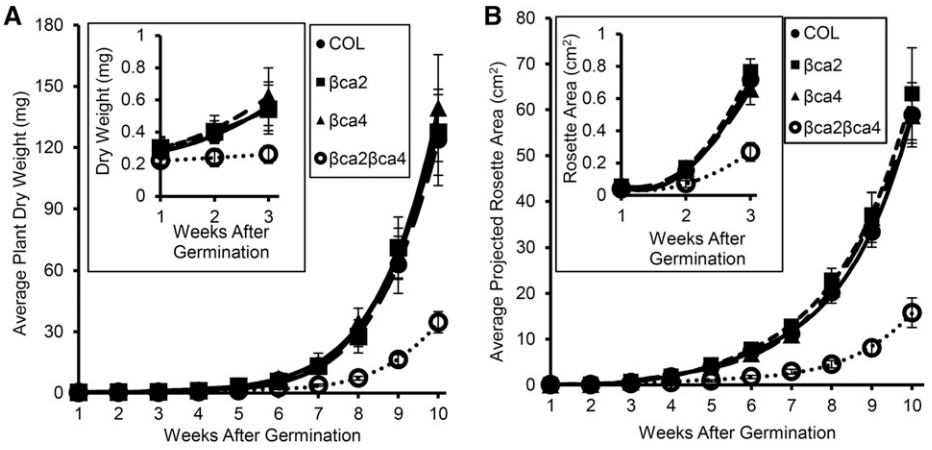

Figure 7. At 200 μL L^{-1} CO_2, *βca2βca4* plants have reduced growth compared with other plant lines. Weekly average aboveground dry weight values (A) and weekly average projected rosette areas (B) show that *βca2βca4* plants grow slower than the other plant lines. Each dry weight symbol represents the mean ± SD of five independent plants. Each symbol for projected rosette area represents the mean ± SD of nine independent plants.

βCA2 coding region in the double mutant restored wild-type growth at low CO_2 (Fig. 9, A and B). Also, the amino acid profile of *βca2βca4 p35S::βCA2* plants resembled the amino acid profile of wild-type plants (data not shown). Genomic PCR showed that T-DNA insertions still disrupted the *βCA2* and *βCA4* genes in the *βca2βca4 p35S::βCA2* plants (Supplemental Fig. S2). Upon further examination, the βCA2 protein was present in the *βca2βca4 p35S::βCA2* plant when using the spinach CA antibody (Fig. 9C). Adding *βCA2* back to *βca2βca4* plants restores normal growth and normal amino acid profiles in low-CO_2 conditions, indicating that this is a CA-facilitated problem.

DISCUSSION

In this work, we present evidence that the two most abundant leaf CAs in the cytoplasm are βCA2 and βCA4. Eliminating either βCA2 or βCA4 produces plants with growth rates that are indistinguishable from the growth rates of wild-type plants (Fig. 6). However, disrupting both βCA2 and βCA4 together resulted in a plant that exhibited slow growth and chlorosis at 200 μL L^{-1} CO_2 and an 8-h photoperiod. The growth of this double mutant was comparable to that of wild-type plants grown at 1,000 μL L^{-1} CO_2. Surprisingly, photosynthesis did not seem to be impaired in the double mutant. However, when the free amino acid content in leaves was measured, the double mutant had significantly lower Asp levels compared with wild-type leaves (Fig. 8). Since 50% of the Asp in the plant is made as a result of PEPC activity (Melzer and O'Leary, 1987), we hypothesize that the loss of βCA2 and βCA4 lowers PEPC activity in the double mutant. Our results are consistent with the amino acid concentrations seen in PEPC knockout plants (Shi et al., 2015) and support the hypothesis that CA activity is required for optimal PEPC activity in the cytoplasm.

Table II. *The slow growth of βca2βca4 is not attributable to lower photosynthetic rates*

The CO_2 compensation points were generated by finding the slope of the initial linear portion of the assimilation/inorganic carbon curve and solving for the *x* intercept. CO_2 assimilation (*A*), stomatal conductance (g_s), and water use efficiency (WUE) values are listed for low (200 μL L^{-1}), ambient (400 μL L^{-1}), and high (1,000 μL L^{-1}) CO_2. Measurements were made with a LI-COR 6400XT gas analyzer using the LI-COR 6400-40 leaf fluorescence cuvette. Values are taken from assimilation/inorganic carbon curves performed on the 16th youngest leaf of four independent 10-week-old plants from each plant line grown in 200 μL L^{-1} CO_2.

Parameter	Wild Type (COL)	*βca2*	*βca4*	*βca2βca4*
CO_2 compensation point	55.9 ± 2.0	53.1 ± 1.4	59.9 ± 4.1	56.4 ± 4.1
200 μL L^{-1} CO_2				
A	4.9 ± 0.32	5.3 ± 0.71	6.3 ± 0.38	5.3 ± 0.90
g_s	0.28 ± 0.04	0.25 ± 0.04	0.37 ± 0.03	0.35 ± 0.04
WUE	0.16 ± 0.02	0.18 ± 0.01	0.15 ± 0.01	0.14 ± 0.01
400 μL L^{-1} CO_2				
A	11.2 ± 1.1	12.1 ± 0.85	13.6 ± 0.6	11.4 ± 1.7
g_s	0.32 ± 0.03	0.29 ± 0.04	0.38 ± 0.03	0.35 ± 0.04
WUE	0.33 ± 0.04	0.35 ± 0.02	0.33 ± 0.01	0.30 ± 0.02
1,000 μL L^{-1} CO_2				
A	18.0 ± 2.1	19.7 ± 1.4	20.8 ± 1.1	18.7 ± 2.2
g_s	0.29 ± 0.04	0.21 ± 0.04	0.38 ± 0.03	0.35 ± 0.04
WUE	0.57 ± 0.12	0.77 ± 0.09	0.51 ± 0.03	0.49 ± 0.02

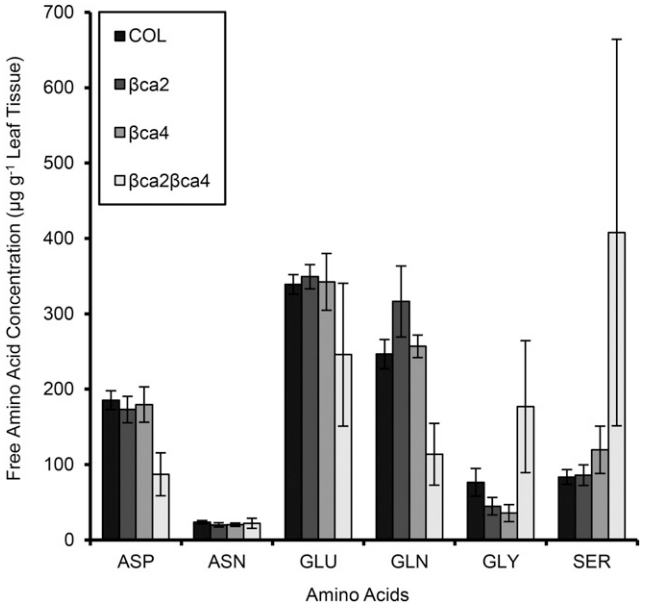

Figure 8. Amino acid concentrations of the wild type (COL), single mutants, and the double mutant. Asp and Gln are reduced significantly in the double mutant, whereas Gly and Ser are elevated in the double mutant. Samples were sent to the TAMU Protein Chemistry Laboratory at Texas A&M University for amino acid analysis. Each bar represents the mean ± SD of three independent plants.

The poor growth of the double mutant but not the single mutants indicates that βCA2 and βCA4 have overlapping functions. One hypothesis examined in this study was that the double mutant grew slowly on low CO_2 because cytoplasmic CA activity is required to facilitate the diffusion of inorganic carbon to the chloroplast for photosynthesis. In this scenario, photosynthesis in the double mutant would be reduced because the CO_2 concentration at Rubisco would be reduced. However, CO_2 assimilation rates in all the mutant lines were similar to values in 10-week-old wild-type plants (Table II). From these measurements, it was concluded that the cytoplasmic CAs do not play an important role in photosynthesis. These observations are in agreement with the models of Badger and Price (1994), Terashima et al., (2011), and Tholen et al. (2012, 2014). They argued that the cytoplasm offers only minimal resistance to CO_2 diffusion because the chloroplasts are often close to the plasma membrane in mesophyll cells.

Another possible role of the cytoplasmic CAs would be to provide HCO_3^- for cytoplasmic PEPC. While PEPC is normally thought to have a very high affinity for inorganic carbon compared with Rubisco, the PEPC K_m (HCO_3^-) has been reported to be between 25 and 100 μM for C_4 plants (O'Leary, 1982; Bauwe, 1986; Hatch and Burnell, 1990) and between 100 and 200 μM for C_3 plants (Mukerji and Yang, 1974; Sato et al., 1988). Since the dissolved CO_2 concentration in the cytoplasm of C_3 plants is expected to be about 12 μM at 400 μL L^{-1} CO_2 and 25°C, the HCO_3^- concentration at equilibrium would be close to 60 μM assuming a cytoplasmic pH of 7 and a CO_2-to-HCO_3^- pKa of 6.4. This estimated HCO_3^- concentration in the cytosol is less than the 100 to 200 μM PEPC K_m (HCO_3^-) for C_3 plants. Therefore, a drop in CO_2 concentration to 200 μL L^{-1} in air would drop the HCO_3^- to about 25 to 30 μM, again well under the

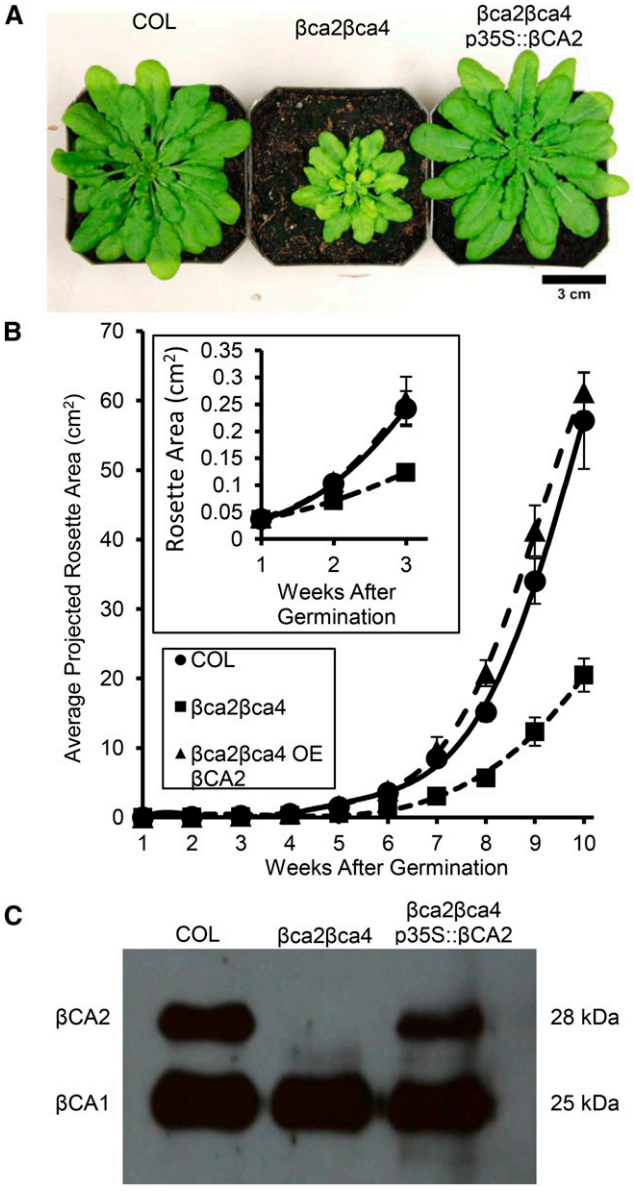

Figure 9. Expressing the βCA2 coding region in *βca2βca4* plants restores wild-type growth in low CO_2. A, Normal growth was restored in *βca2βca4 p35S::βCA2* plants growing at 200 μL L^{-1} CO_2. All plants were grown under an 8-h-light (22°C)/16-h-dark (18°C) regime with a light intensity of 120 μmol photons m^{-2} s^{-1}. B, Weekly average projected rosette areas for each line show that normal growth was restored in the double mutant by adding *p35S::βCA2*. Each symbol represents the mean ± SD of nine individual plants per line. C, Western blotting shows the presence of the βCA2 protein restored in the *βca2βca4 p35S::βCA2* plants. Each lane contains 5 μg μL^{-1} total protein extract from leaves of wild-type (COL), *βca2βca4*, and *βca2βca4 p35S::βCA2* plants.

reported K_m (HCO_3^-) for PEPC. It is estimated that 50% of carbon at position 4 in Asp can be attributed to PEPC activity (Melzer and O'Leary, 1987); therefore, we measured Asp levels in wild-type plants, the single mutants, and the double mutant (Fig. 8; Supplemental Table S1). The wild-type and single mutant plants had similar amino acid profiles, with Asp levels between 173 and 185 $\mu g\ g^{-1}$ leaf tissue. In contrast, the Asp level in the double mutant was only 87 $\mu g\ g^{-1}$ leaf tissue, while the mean Gly and Ser levels in the double mutant were severalfold higher than the mean levels in wild-type and single mutant plants (Fig. 8). In a previous study of a knockout of two PEPCs, a similar profile of low levels of Asp and high levels of Gly and Ser was found (Shi et al., 2015). Like the *βca2βca4* double mutant (Fig. 6), the PEPC double mutant showed reduced growth and chlorosis (Shi et al., 2015).

The results reported here also clarify the gene models for *βCA2* and *βCA4*. Previously, only βCA2 (Fett and Coleman, 1994; Fabre et al., 2007) and βCA3 (Fabre et al., 2007) were reported to be in the cytoplasm. The only reports for βCA4 localization indicated that the protein was associated with the plasma membrane (Fabre et al., 2007; Hu et al., 2010, 2015). In addition, we found the gene models presented in TAIR to be incomplete for *βCA4* and inaccurate for *βCA2*. For *βCA2*, the gene models all show an exon/intron pattern very similar to that for *βCA1* and predict that *βCA2* should localize in the chloroplast. However, RNAseq data (Fig. 1) and deposited ESTs show that more than 95% of the *βCA2* transcripts begin in the middle of the second exon in the TAIR model. This is consistent with a *βCA2* mRNA that encodes a cytoplasmic protein, because the chloroplast transit peptide would be omitted (Fett and Coleman, 1994; Fabre et al., 2007). The mature βCA1 protein without its chloroplast transit peptide is smaller than the mature βCA2 protein (Supplemental Fig. S1), further supporting a cytoplasmic localization for βCA2. Abundant GUS staining is seen in the leaf when GUS is linked to a promoter made immediately upstream of the ATG start site for the predicted cytoplasmic βCA2 (Fig. 2). This GUS expression pattern for *βCA2* coincides with the leaf CA activity levels reported in pea (*Pisum sativum*; Majeau and Coleman, 1994) and bean (*Phaseolus vulgaris*; Porter and Grodzinski, 1984) and also fits with the observed EST abundance in TAIR microarray data (Schmid et al., 2005; Winter et al., 2007; Ferreira et al., 2008) as well as RNAseq data (Table I). Our results are in contrast to those of Wang et al. (2014), who observed little or no GUS staining in the leaf with their *βCA2* promoter. However, they used a sequence upstream of the first exon of the TAIR gene model, and our data and the EST data indicate that the first exon in the TAIR model is transcribed at a very low level, if at all.

The gene model for *βCA4* is somewhat complex. There are two different and abundant transcripts made from the *βCA4* gene in the leaf, *βCA4.1* and *βCA4.2* (Table I; Fig. 1). The longer leaf transcript, *βCA4.1*, encodes a protein that is targeted to the plasma membrane, as shown by our localization studies and the published work of Fabre et al. (2007) and Hu et al., (2010, 2015). Here, we also determined that *βCA4.2*, the shorter transcript, encodes a cytoplasmic CA (Figs. 3 and 4). The RNAseq data also show that *βCA4.2* transcripts are found in the roots while both *βCA4.1* and *βCA4.2* transcripts are found in leaf tissue. GUS expression studies (Fig. 2) are consistent with the RNAseq data (Figs. 1 and 2). When a *βCA4.2* promoter (Fig. 2B) was linked to GUS, only root expression was observed (Fig. 2C). A more complete promoter linked to GUS showed both root and leaf expression (Fig. 2, B and C). However, we were unable to find a *βCA4.1* promoter sequence that showed expression only in leaves (data not shown). Other studies have found multiple transcripts of *βCA4* (Aubry et al., 2014; Wang et al., 2014), but, to our knowledge, this is the first report showing that the different *βCA4* transcripts encode proteins with different destinations in the cell.

RNAseq data and earlier microarray and expression studies show that *βCA2* and *βCA4* are highly expressed in leaves, whereas *βCA3* is expressed at less than 5% of the level of either *βCA2* or *βCA4* (Table I; Schmid et al., 2005; Fabre et al., 2007; Winter et al., 2007; Ferreira et al., 2008). In addition, Hu et al. (2010) presented evidence showing high expression of *βCA2* and *βCA4* in mesophyll cells, whereas *βCA3* had very low expression in mesophyll cells, while Wang et al. (2014) reported very low *βCA3* expression in leaves with promoter::GUS studies. Since the other CAs that show significant expression are either in the chloroplast (Fett and Coleman, 1994; Villarejo et al., 2005; Fabre et al., 2007; Burén et al., 2011; Hu et al., 2015) or mitochondria (Fabre et al., 2007; Jiang et al., 2014), we conclude that βCA2 and βCA4 are the most abundant CA isoforms in the cytoplasm. This contention is supported by leaf RNAseq data (Table I), GUS staining (Fig. 2), CA microarray analysis (Ferreira et al., 2008), as well as publicly available EST and microarray data (Schmid et al., 2005; Winter et al., 2007).

Previously, researchers lowered the expression of the chloroplastic CA, βCA1 (Majeau et al., 1994; Price et al., 1994; Ferreira et al., 2008), and found normal growth and carbon assimilation rates in plants with reduced βCA1. More recently, Jiang et al. (2014) reported that plants lacking the mitochondrial βCA6 grew slowly on low CO_2. There have been few studies of other CA isoforms. A notable exception has been the construction of double and triple mutant lines of the most abundant CAs in leaf guard cells, including βCA1, βCA4, and βCA6 (Hu et al., 2010, 2015; Xue et al., 2011). These CAs are localized to different organelles in the guard cell, with βCA1 located in the chloroplast, βCA4 in the plasma membrane, and βCA6 in the mitochondria. Eliminating the expression of these guard cell CAs caused changes in stomatal density and temporal changes in stomatal conductance in response to changes in CO_2 level or humidity (Hu et al., 2010; Engineer et al., 2014), leading to the hypothesis that CA activity is an important factor in how plant guard cells

sense CO_2 concentration (Xue et al., 2011). In this study, stomatal density was unaffected by knocking out cytosolic βCA2 and/or βCA4 (Supplemental Fig. S3).

In conclusion, we show evidence that βCA2 and βCA4 are the most abundant cytoplasmic CAs in Arabidopsis leaves. The loss of both of these proteins reduced growth at low CO_2 concentration. We hypothesize that βCA2 and βCA4 are necessary for the proper function of cytosolic PEPC needed for the production of amino acids. It is also likely that the large number of CA genes and isoforms in plants indicates that CA may be needed for a number of metabolic pathways in different tissues.

MATERIALS AND METHODS

Plant Lines and Growth Conditions

Arabidopsis (*Arabidopsis thaliana*) plants of the COL ecotype were used in this study. The T-DNA lines, *βca2* (SALK_145785) and *βca4* (CS859392), were obtained from TAIR and backcrossed into wild-type (COL) three times before allowing the selfing of heterozygous mutants to produce the homozygous mutant lines used in this study. The double mutant, *βca2βca4*, was generated by crossing the backcrossed homozygous *βca2* line with the backcrossed homozygous *βca4* line. These plants were grown in a Percival AR-66L growth chamber either at low CO_2 (200 μL L^{-1}) or high CO_2 (1,000 μL L^{-1}) in a short-day photoperiod of 8 h of light (22°C)/16 h of dark (18°C) at a light intensity of 120 μmol photons m^{-2} s^{-1}. Plants were watered biweekly, alternating between distilled water and a 1:3 dilution of Hoagland nutrient solution in distilled water (Epstein and Bloom, 2005).

GUS, eGFP, and Complementation T-DNA Vector Construction

Primers for amplifying the various regions of DNA or complementary DNA (cDNA) that were inserted into the pENTR/D-TOPO cloning vector were designed using the Integrated DNA Technologies primer design Web page and were generated by Integrated DNA Technologies. Cloning primers are listed in Supplemental Table S2. Coding regions of the *βCA1* (At3g01500), *βCA2* (At5g14740), and *βCA4* (At1g70410) genes were amplified from the cDNA vectors obtained from TAIR, U17263, U09011, and U09528, respectively. The CA coding regions used for eGFP fluorescence were amplified from the ATG start codon to the codon directly 5′ of the stop codon. CA coding regions used for complementation studies also were amplified starting from the ATG start codon, but these amplicons included the stop codon. CA promoter regions to drive GUS expression were amplified using genomic DNA isolated from COL plant leaves. In most cases, the promoter regions amplified contained DNA fragments that included the entire 5′ untranslated region of the CA gene and continued into the gene directly upstream of the CA gene. Amplicons used for cloning were obtained by PCR amplification. PCR steps included an initial 98°C denaturation step for 3 min, 35 cycles of 98°C for 30 s, annealing temperature for 30 s, and 72°C set for 20 s per 1,000 bases, a final 72°C step for 5 min, and a holding temperature of 4°C. Phusion DNA polymerase (New England Biolabs) and the Bio-Rad T100 Thermal Cycler were used for DNA amplification. Amplicons were gel purified following the procedure of the Qiaquick Gel Purification kit (Qiagen). Purified amplicons were cloned into the pENTR/D-TOPO vector following the kit procedure (Invitrogen). The correct sequence and orientation of the amplicons in the pENTR vector were confirmed by sequencing the pENTR clones. eGFP amplicons were recombined into the pDEST vector pB7FWG2 (Karimi et al., 2002), complementation amplicons were recombined into the pDEST vector pMDC32 (Curtis and Grossniklaus, 2003), and GUS amplicons were recombined into the pDEST vector pKGWFS7 (Karimi et al., 2002) following the Gateway LR Clonase kit procedure (Invitrogen). The correct orientation of the amplicon in the pDEST vector was confirmed via restriction digestion. Correctly generated pDEST vectors were transformed into the *Agrobacterium tumefaciens* strain GV3101 using a freeze-thaw protocol as described (Weigel and Glazebrook, 2002).

A. tumefaciens Transfection and Screening of Transformants

Stable eGFP, GUS, and complementation lines were created following a modified procedure (Weigel and Glazebrook, 2002). A total of 200 μL of transformed *A. tumefaciens* was used to inoculate 200 mL of YEP medium supplemented with antibiotics (30 μg mL^{-1} gentamycin and 10 μg mL^{-1} rifampicin for *A. tumefaciens* helper plasmids and either 100 μg mL^{-1} spectinomycin for the eGFP and GUS vectors or 50 μg mL^{-1} kanamycin for the complementation vector). The cultures were grown overnight at 28°C with vigorous shaking, and cells were pelleted in the morning by centrifugation at 6,000 rpm using a Beckman J2-HS centrifuge and JA-10 rotor. Pelleted cells were resuspended in 400 mL of *A. tumefaciens* infiltration medium (one-half-strength Murashige and Skoog medium with Gamborg's vitamins from Caisson Laboratories, 5% [w/v] Suc, 0.044 μM benzylaminopurine suspended in dimethyl sulfoxide, and 50 μL L^{-1} Silwet L-77 from Lehle Seeds). Stalks of Arabidopsis (COL) plants were dipped in the *A. tumefaciens* infiltration medium for approximately 40 s and then laid sideways in a flat with a covered dome to recover overnight, incubating in constant light at 21°C (Weigel and Glazebrook, 2002). eGFP transformants were selected on soil by spraying seedlings with a 1:1,000 dilution of BASTA (AgrEvo), whereas GUS or complementation transformants were selected on one-half-strength Murashige and Skoog plates (pH 6) with no Suc supplemented with 50 μg mL^{-1} kanamycin or 20 μg mL^{-1} hygromycin, respectively.

Histochemical GUS Staining

At least five independently transformed plants that showed stable GUS expression through three generations were used for this study. GUS staining was performed following the protocol from Jefferson et al. (1987). Three-week-old plants were vacuum infiltrated for 5 min with a GUS staining solution [0.1 M $NaPO_4$, pH 7, 10 mM EDTA, 0.1% (v/v) Triton X-100, 1 mM $K_3Fe(CN)_6$, and 2 mM 5-bromo-4-chloro-3-indolyl-β-D-GlcA (from GoldBio) suspended in *N*,*N*-dimethylformamide] and placed in the dark in a 37°C incubator overnight. The GUS staining solution was removed the following morning, and plant tissues were incubated in 100% (v/v) methanol at 60°C for 15 min repeatedly until all chlorophyll was removed. Plants were photographed with a Canon EOS Rebel T5i camera with the Canon EF 100mm f/2.8L macro IS USM lens.

Protoplast Preparation and eGFP Visualization

At least four independently transformed eGFP lines showing stable eGFP expression over three generations were used for this study. Following the protocol of Wu et al. (2009), 2 g of leaf tissue was incubated in 10 mL of enzyme solution (1% [w/v] cellulase from *Trichoderma viride* [Sigma], 0.25% [w/v] pectinase from *Rhizopus* spp. [Sigma], 0.4 M mannitol, 10 mM $CaCl_2$, 20 mM KCl, 0.1% [w/v] bovine serum albumin, and 20 mM MES at pH 5.7) for 1 h in light after placing Time Tape on the upper epidermis of the leaves and removing the lower epidermis of the leaves via Magic Tape. Protoplasts were then pelleted by centrifugation at 800 rpm for 3 min using a Beckman J2-HS centrifuge and JS-13.1 rotor. Protoplasts were resuspended in a solution containing 0.4 M mannitol, 15 mM $MgCl_2$, and 4 mM MES at pH 5.7. Stably expressing eGFP leaves were prepared for confocal imaging by removing an approximately 0.75-cm^2 leaf sample and incubating it in a welled-microscope slide filled with 100 μL of perfluorodecalin (Sigma) for 5 min (Littlejohn and Love, 2012). eGFP fluorescence was visualized using protoplasts and prepared leaves from stable eGFP plants with a Leica SP2 confocal microscope. A 40× oil-emersion lens was used to visualize protoplasts and a 20× objective lens was used to visualize intact cells from leaf samples. eGFP and chlorophyll were excited using a krypton/argon laser tuned to 488 nm, and eGFP and chlorophyll fluorescence were observed between the wavelengths of 500 to 520 nm and 660 to 700 nm, respectively.

Genotyping T-DNA Lines Using Genomic PCR and Reverse Transcription-PCR

DNA for genomic PCR was isolated from Arabidopsis leaves ground with a mortar and pestle and incubated in Edward's extraction buffer (200 mM Tris-Cl, pH 7.5, 250 mM NaCl, 25 mM EDTA, and 0.5% [w/v] SDS). DNA was precipitated using 100% (v/v) isopropanol and 70% (v/v) ethanol washes. One hundred nanograms of DNA was used in a genomic PCR using the standard protocol for One Taq (New England Biolabs). Primers used for each reaction can

be found in Supplemental Table S2. RNA for reverse transcription was isolated from 80 mg of leaf tissue from 6-week-old Arabidopsis plants grown in low CO_2 and short days using the Qiagen RNeasy Plant minikit. Three micrograms of RNA was used for the reverse transcription reaction, and cDNA was generated using the SuperScript First-Strand RT-PCR kit and protocol (Invitrogen). cDNA at 0.5 μL was used for a 25-μL PCR using the standard protocol for One Taq (New England Biolabs).

RNAseq Analysis

RNAseq reads were generated and processed to calculate expression counts as described by Oh et al. (2014). An average count from three biological replicates was used in this study.

Western Blotting of βCA2

Protein was extracted from 50 mg of fresh Arabidopsis leaf tissue. Ground leaf samples were incubated in a protein extraction buffer (1× TE, 1.2% [w/v] SDS, 2.7% [w/v] Suc, and 7.5 μg mL^{-1} Bromophenol Blue) on ice for 15 min and then centrifuged for 5 min at 14,000 rpm to pellet the cell debris. The supernatant was collected and used for protein quantification following the Bradford assay protocol (Pierce). 2-Mercaptoethanol was added to a final concentration of 350 mM in the supernatant, and the protein samples were incubated at 100°C for 3 min. Five micrograms of protein from each sample was loaded onto a 12% (w/v) acrylamide gel and allowed to separate before transferring to a polyvinylidene difluoride (PVDF) membrane (Bio-Rad). The PVDF membrane was blocked in 5% (w/v) dry milk for 1 h before it was washed with a TTBS solution (0.05% [v/v] Tween 20, 19 mM Tris base, and 500 mM NaCl, pH 7.5) three times. The PVDF membrane was incubated with a 1:20,000 dilution of a spinach (*Spinacia oleracea*) CA polyclonal antibody (Fawcett et al., 1990) in a TBSB solution (1% [w/v] bovine serum albumin, 19 mM Tris base, and 500 mM NaCl, pH 7.5) overnight at 4°C. The following morning, the membrane was washed five times with TTBS to remove the primary antibody and then was incubated in a 1:20,000 dilution of the Bio-Rad goat anti-rabbit secondary antibody in TBSB for 1 h at room temperature. The membrane was subjected to five more washes of TTBS to remove excess secondary antibody before incubation in a 1:1 mixture of peroxide and luminol (Bio-Rad). Protein bands were visualized on x-ray film via chemiluminescence.

Rosette Area and Dry Weight Measurements

To obtain rosette areas of the various lines grown at 200 μL L^{-1} CO_2, images of each plant line were taken weekly using a Canon Rebel T5i camera with a Canon 15-85mm f/3.5-5.6 IS USM lens. Rosette areas were attained by tracing the outlines of the plants and obtaining the projected rosette area within each outline in ImageJ (National Institutes of Health). Projected rosette areas were measured on nine plants per line. Dry weights of aboveground plant mass were measured every week for each plant line for 10 weeks. Five plants per line were used for dry weight analysis. Plant rosettes were clipped at the crown of the plant and incubated in an oven at 60°C. Dry weight measurements were conducted once per day until plant dry weights stabilized.

Gas-Exchange Measurements

Photosynthesis measurements were conducted using the LI-COR 6400XT gas analyzer. Plants used for gas-exchange measurements were grown at 200 μL L^{-1} CO_2 for 10 weeks and then shifted to 1,000 μL L^{-1} CO_2 for 2 weeks in order to obtain leaves big enough from the *βca2βca4* line to fill the LI-COR 6400-40 leaf fluorescence cuvette. Before photosynthesis measurements were taken on an Arabidopsis leaf, the leaf was allowed to acclimate to 400 μL L^{-1} CO_2 and 1,000 μmol photons m^{-2} s^{-1} (saturating irradiance for these leaves) for 1 h or until steady-state photosynthesis rates were attained. CO_2 assimilation/inorganic carbon curves were measured on the 16th youngest leaf from four separate plants of each plant line. Each curve started at 400 μL L^{-1} CO_2 and decreased to 50 μL L^{-1} CO_2 before returning to 400 μL L^{-1} CO_2 and subsequently increasing to 2,200 μL L^{-1} CO_2. For each CO_2 point, individual leaves reached steady-state photosynthesis within 3 min on average before measurements were recorded.

Complementation of the *βca2βca4* Mutant

The coding region of βCA2 was recombined into the Gateway overexpression vector pMDC32 (Curtis and Grossniklaus, 2003), creating the construct *p35S::βCA2*. This vector was transformed into the *A. tumefaciens* strain GV3101 using the freeze-thaw method (Weigel and Glazebrook, 2002) and then stably transformed into the *βca2βca4* line via the floral dip technique (Weigel and Glazebrook, 2002). Transformants were selected on one-half-strength Murashige and Skoog plates supplemented with 30 μg mL^{-1} hygromycin and then transferred to soil after 3 weeks of growth on plates. These transformants produced seeds that were used to compare the growth of wild-type (COL), *βca2βca4*, and *βca2βca4 p35S::βCA2* plants in low CO_2 (200 μL L^{-1} CO_2).

Leaf Amino Acid Analysis

One hundred milligrams of leaf tissue was harvested from 6-week-old plants grown in low CO_2 (200 μL L^{-1} CO_2). The leaf tissue was immediately frozen in liquid N_2 and ground with a mortar and pestle. Five hundred microliters of 80% (v/v) methanol was added to the ground leaf tissue, and each sample was incubated at 75°C for 10 min. Samples were then centrifuged at 20,000*g* for 5 min at 4°C using a Beckman centrifuge and JA-18.1 rotor. The supernatant was collected, and 500 μL of 20% (v/v) methanol was added to resuspend the pellet. Samples were centrifuged again, and the two supernatants were combined and pulled through a 0.2-μm filter (VWR International). Three biological replicates of each plant line were quantified using the protocol from Lowry et al. (1951) and shipped to the TAMU Protein Chemistry Laboratory at Texas A&M University for amino acid analysis.

RNAseq data can be retrieved from the National Center for Biotechnology Information Sequence Read Archive database as BioSample:SAMN03339724.

Supplemental Data

The following supplemental materials are available.

Supplemental Figure S1. Western blot confirming that the CA antibody cross-reacts with both βCA1 and βCA2.

Supplemental Figure S2. Genomic PCR probing for the *p35S::βCA2* construct in the *βca2βca4* mutant.

Supplemental Figure S3. Lacking cytosolic CAs does not alter the stomatal density of the double mutant.

Supplemental Table S1. Total amino acid amounts obtained from the amino acid analysis performed on wild-type, single mutant, and double mutant leaves.

Supplemental Table S2. List of all primer sets used to genotype plant lines and generate constructs for GUS analysis, GFP fluorescence, and complementation studies.

ACKNOWLEDGMENTS

We thank Bernard Genty for many helpful discussions and Sue Bartlett for the anti-spinach CA antibody.

Received December 23, 2015; accepted March 16, 2016; published March 18, 2016.

LITERATURE CITED

Aubry S, Smith-Unna RD, Boursnell CM, Kopriva S, Hibberd JM (2014) Transcript residency on ribosomes reveals a key role for the Arabidopsis thaliana bundle sheath in sulfur and glucosinolate metabolism. Plant J **78:** 659–673

Badger MR, Price GD (1994) The role of carbonic-anhydrase in photosynthesis. Annu Rev Plant Physiol Plant Mol Biol **45:** 369–392

Bauwe H (1986) An efficient method for the determination of K_m values for HCO_3^- of phosphoenolpyruvate carboxylase. Planta **169:** 356–360

Bracey MH, Christiansen J, Tovar P, Cramer SP, Bartlett SG (1994) Spinach carbonic anhydrase: investigation of the zinc-binding ligands by site-directed mutagenesis, elemental analysis, and EXAFS. Biochemistry **33:** 13126–13131

Burén S, Ortega-Villasante C, Blanco-Rivero A, Martínez-Bernardini A, Shutova T, Shevela D, Messinger J, Bako L, Villarejo A, Samuelsson G (2011) Importance of post-translational modifications for functionality of

a chloroplast-localized carbonic anhydrase (CAH1) in Arabidopsis thaliana. PLoS ONE **6:** e21021

Cuesta-Seijo JA, Borchert MS, Navarro-Poulsen JC, Schnorr KM, Mortensen SB, Lo Leggio L (2011) Structure of a dimeric fungal α-type carbonic anhydrase. FEBS Lett **585:** 1042–1048

Curtis MD, Grossniklaus U (2003) A Gateway cloning vector set for high-throughput functional analysis of genes in planta. Plant Physiol **133:** 462–469

Engineer CB, Ghassemian M, Anderson JC, Peck SC, Hu H, Schroeder JI (2014) Carbonic anhydrases, EPF2 and a novel protease mediate CO_2 control of stomatal development. Nature **513:** 246–250

Epstein E, Bloom AJ (2005) Mineral Nutrition of Plants: Principles and Perspectives, Ed 2. Sinauer Associates, Sunderland, MA, p 31

Fabre N, Reiter IM, Becuwe-Linka N, Genty B, Rumeau D (2007) Characterization and expression analysis of genes encoding alpha and beta carbonic anhydrases in Arabidopsis. Plant Cell Environ **30:** 617–629

Fawcett TW, Browse JA, Volokita M, Bartlett SG (1990) Spinach carbonic anhydrase primary structure deduced from the sequence of a cDNA clone. J Biol Chem **265:** 5414–5417

Ferreira FJ, Guo C, Coleman JR (2008) Reduction of plastid-localized carbonic anhydrase activity results in reduced Arabidopsis seedling survivorship. Plant Physiol **147:** 585–594

Fett JP, Coleman JR (1994) Characterization and expression of two cDNAs encoding carbonic anhydrase in *Arabidopsis thaliana*. Plant Physiol **105:** 707–713

Grigoriev IV, Nordberg H, Shabalov I, Aerts A, Cantor M, Goodstein D, Kuo A, Minovitsky S, Nikitin R, Ohm RA, et al (2012) The genome portal of the Department of Energy Joint Genome Institute. Nucleic Acids Res **40:** D26–D32

Hatch MD, Burnell JN (1990) Carbonic anhydrase activity in leaves and its role in the first step of C_4 photosynthesis. Plant Physiol **93:** 825–828

Hewett-Emmett D, Tashian RE (1996) Functional diversity, conservation, and convergence in the evolution of the α-, β-, and γ-carbonic anhydrase gene families. Mol Phylogenet Evol **5:** 50–77

Hilvo M, Baranauskiene L, Salzano AM, Scaloni A, Matulis D, Innocenti A, Scozzafava A, Monti SM, Di Fiore A, De Simone G, et al (2008) Biochemical characterization of CA IX, one of the most active carbonic anhydrase isozymes. J Biol Chem **283:** 27799–27809

Hoang CV, Chapman KD (2002) Biochemical and molecular inhibition of plastidial carbonic anhydrase reduces the incorporation of acetate into lipids in cotton embryos and tobacco cell suspensions and leaves. Plant Physiol **128:** 1417–1427

Hu H, Boisson-Dernier A, Israelsson-Nordström M, Böhmer M, Xue S, Ries A, Godoski J, Kuhn JM, Schroeder JI (2010) Carbonic anhydrases are upstream regulators of CO_2-controlled stomatal movements in guard cells. Nat Cell Biol **12:** 87–93, 1–18

Hu H, Rappel WJ, Occhipinti R, Ries A, Böhmer M, You L, Xiao C, Engineer CB, Boron WF, Schroeder JI (2015) Distinct cellular locations of carbonic anhydrases mediate carbon dioxide control of stomatal movements. Plant Physiol **169:** 1168–1178

Iverson TM, Alber BE, Kisker C, Ferry JG, Rees DC (2000) A closer look at the active site of gamma-class carbonic anhydrases: high-resolution crystallographic studies of the carbonic anhydrase from Methanosarcina thermophila. Biochemistry **39:** 9222–9231

Jefferson RA, Kavanagh TA, Bevan MW (1987) GUS fusions: beta-glucuronidase as a sensitive and versatile gene fusion marker in higher plants. EMBO J **6:** 3901–3907

Jiang CY, Tholen D, Xu JM, Xin CP, Zhang H, Zhu XG, Zhao YX (2014) Increased expression of mitochondria-localized carbonic anhydrase activity resulted in an increased biomass accumulation in Arabidopsis thaliana. J Plant Biol **57:** 366–374

Karimi M, Inzé D, Depicker A (2002) GATEWAY vectors for Agrobacterium-mediated plant transformation. Trends Plant Sci **7:** 193–195

Kawahara Y, de la Bastide M, Hamilton JP, Kanamori H, McCombie WR, Ouyang S, Schwartz DC, Tanaka T, Wu J, Zhou S, et al (2013) Improvement of the Oryza sativa Nipponbare reference genome using next generation sequence and optical map data. Rice (N Y) **6:** 4

Kim HJ (1997) Identification of the physiological role of carbonic anhydrase using the antisense technique and investigation of its transcriptional regulation in *Arabidopsis thaliana* (L.) Heynh. PhD thesis. Louisiana State University, Baton Rouge

Kimber MS, Pai EF (2000) The active site architecture of Pisum sativum beta-carbonic anhydrase is a mirror image of that of alpha-carbonic anhydrases. EMBO J **19:** 1407–1418

Kisker C, Schindelin H, Alber BE, Ferry JG, Rees DC (1996) A left-hand beta-helix revealed by the crystal structure of a carbonic anhydrase from the archaeon Methanosarcina thermophila. EMBO J **15:** 2323–2330

Liljas A, Kannan KK, Bergstén PC, Waara I, Fridborg K, Strandberg B, Carlbom U, Järup L, Lövgren S, Petef M (1972) Crystal structure of human carbonic anhydrase C. Nat New Biol **235:** 131–137

Littlejohn GR, Love J (2012) A simple method for imaging *Arabidopsis* leaves using perfluorodecalin as an infiltrative imaging medium. J Vis Exp **59:** 3394

Lowry OH, Rosebrough NJ, Farr AL, Randall RJ (1951) Protein measurement with the Folin phenol reagent. J Biol Chem **193:** 265–275

Majeau N, Arnoldo MA, Coleman JR (1994) Modification of carbonic anhydrase activity by antisense and over-expression constructs in transgenic tobacco. Plant Mol Biol **25:** 377–385

Majeau N, Coleman JR (1994) Correlation of carbonic-anhydrase and ribulose-1,5-bisphosphate carboxylase/oxygenase expression in pea. Plant Physiol **104:** 1393–1399

Martin V, Villarreal F, Miras I, Navaza A, Haouz A, González-Lebrero RM, Kaufman SB, Zabaleta E (2009) Recombinant plant gamma carbonic anhydrase homotrimers bind inorganic carbon. FEBS Lett **583:** 3425–3430

Melzer E, O'Leary MH (1987) Anapleurotic CO_2 fixation by phosphoenolpyruvate carboxylase in C_3 plants. Plant Physiol **84:** 58–60

Moroney JV, Bartlett SG, Samuelsson G (2001) Carbonic anhydrases in plants and algae. Plant Cell Environ **24:** 141–153

Mukerji SK, Yang SF (1974) Phosphoenolpyruvate carboxylase from spinach leaf tissue: inhibition by sulfite ion. Plant Physiol **53:** 829–834

Oh DH, Hong H, Lee SY, Yun DJ, Bohnert HJ, Dassanayake M (2014) Genome structures and transcriptomes signify niche adaptation for the multiple-ion-tolerant extremophyte Schrenkiella parvula. Plant Physiol **164:** 2123–2138

O'Leary MH (1982) Phosphoenolpyruvate carboxylase: an enzymologist's view. Annu Rev Plant Physiol **33:** 297–315

Perales M, Parisi G, Fornasari MS, Colaneri A, Villarreal F, González-Schain N, Echave J, Gómez-Casati D, Braun HP, Araya A, et al (2004) Gamma carbonic anhydrase like complex interact with plant mitochondrial complex I. Plant Mol Biol **56:** 947–957

Porter MA, Grodzinski B (1984) Acclimation to high CO_2 in bean: carbonic-anhydrase and ribulose bisphosphate carboxylase. Plant Physiol **74:** 413–416

Price GD, Voncaemmerer S, Evans JR, Yu JW, Lloyd J, Oja V, Kell P, Harrison K, Gallagher A, Badger MR (1994) Specific reduction of chloroplast carbonic-anhydrase activity by antisense RNA in transgenic tobacco plants has a minor effect on photosynthetic CO_2. Planta **193:** 331–340

Raven J, Newman J (1994) Requirement for carbonic anhydrase activity in processes other than photosynthetic inorganic carbon assimilation. Plant Cell Environ **17:** 123–130

Sato F, Koizumi N, Yamada Y (1988) Purification and characterization of phosphoenolpyruvate carboxylase of photomixotrophically cultured green tobacco cells. Plant Cell Physiol **29:** 329–337

Schmid M, Davison TS, Henz SR, Pape UJ, Demar M, Vingron M, Schölkopf B, Weigel D, Lohmann JU (2005) A gene expression map of Arabidopsis thaliana development. Nat Genet **37:** 501–506

Shi J, Yi K, Liu Y, Xie L, Zhou Z, Chen Y, Hu Z, Zheng T, Liu R, Chen Y, et al (2015) Phospho*enol*pyruvate carboxylase in Arabidopsis leaves plays a crucial role in carbon and nitrogen metabolism. Plant Physiol **167:** 671–681

Soto D, Córdoba JP, Villarreal F, Bartoli C, Schmitz J, Maurino VG, Braun HP, Pagnussat GC, Zabaleta E (2015) Functional characterization of mutants affected in the carbonic anhydrase domain of the respiratory complex I in Arabidopsis thaliana. Plant J **83:** 831–844

Studer AJ, Gandin A, Kolbe AR, Wang L, Cousins AB, Brutnell TP (2014) A limited role for carbonic anhydrase in C4 photosynthesis as revealed by a *ca1ca2* double mutant in maize. Plant Physiol **165:** 608–617

Sunderhaus S, Dudkina NV, Jänsch L, Klodmann J, Heinemeyer J, Perales M, Zabaleta E, Boekema EJ, Braun HP (2006) Carbonic anhydrase subunits form a matrix-exposed domain attached to the membrane arm of mitochondrial complex I in plants. J Biol Chem **281:** 6482–6488

Suzuki K, Shimizu S, Juan ECM, Miyamoto T, Fang Z, Hoque MM, Sato Y, Tsunoda M, Sekiguchi T, Takénaka A, et al (2010) Crystallographic study of wild-type carbonic anhydrase α CA1 from Chlamydomonas

reinhardtii. Acta Crystallogr Sect F Struct Biol Cryst Commun **66:** 1082–1085

Suzuki K, Yang SY, Shimizu S, Morishita EC, Jiang J, Zhang F, Hoque MM, Sato Y, Tsunoda M, Sekiguchi T, et al (2011) The unique structure of carbonic anhydrase αCA1 from Chlamydomonas reinhardtii. Acta Crystallogr D Biol Crystallogr **67:** 894–901

Terashima I, Hanba YT, Tholen D, Niinemets Ü (2011) Leaf functional anatomy in relation to photosynthesis. Plant Physiol **155:** 108–116

Tholen D, Ethier G, Genty B (2014) Mesophyll conductance with a twist. Plant Cell Environ **37:** 2456–2458

Tholen D, Ethier G, Genty B, Pepin S, Zhu XG (2012) Variable mesophyll conductance revisited: theoretical background and experimental implications. Plant Cell Environ **35:** 2087–2103

Tobin AJ (1970) Carbonic anhydrase from parsley leaves. J Biol Chem **245:** 2656–2666

Villarejo A, Burén S, Larsson S, Déjardin A, Monné M, Rudhe C, Karlsson J, Jansson S, Lerouge P, Rolland N, et al (2005) Evidence for a protein transported through the secretory pathway en route to the higher plant chloroplast. Nat Cell Biol **7:** 1224–1231

Villarreal F, Martín V, Colaneri A, González-Schain N, Perales M, Martín M, Lombardo C, Braun HP, Bartoli C, Zabaleta E (2009) Ectopic expression of mitochondrial gamma carbonic anhydrase 2 causes male sterility by anther indehiscence. Plant Mol Biol **70:** 471–485

von Caemmerer S, Quinn V, Hancock NC, Price GD, Furbank RT, Ludwig M (2004) Carbonic anhydrase and C-4 photosynthesis: a transgenic analysis. Plant Cell Environ **27:** 697–703

Wang M, Zhang Q, Liu FC, Xie WF, Wang GD, Wang J, Gao QH, Duan K (2014) Family-wide expression characterization of Arabidopsis beta-carbonic anhydrase genes using qRT-PCR and promoter:GUS fusions. Biochimie **97:** 219–227

Weigel D, Glazebrook J (2002) How to transform Arabidopsis. *In* Arabidopsis: A Laboratory Manual. Cold Spring Harbor Laboratory Press, Cold Spring Harbor, NY, pp 119–141

Whittington DA, Waheed A, Ulmasov B, Shah GN, Grubb JH, Sly WS, Christianson DW (2001) Crystal structure of the dimeric extracellular domain of human carbonic anhydrase XII, a bitopic membrane protein overexpressed in certain cancer tumor cells. Proc Natl Acad Sci USA **98:** 9545–9550

Williams TG, Flanagan LB, Coleman JR (1996) Photosynthetic gas exchange and discrimination against $^{13}CO_2$ and $C^{18}O^{16}O$ in tobacco plants modified by an antisense construct to have low chloroplastic carbonic anhydrase. Plant Physiol **112:** 319–326

Winter D, Vinegar B, Nahal H, Ammar R, Wilson GV, Provart NJ (2007) An "Electronic Fluorescent Pictograph" browser for exploring and analyzing large-scale biological data sets. PLoS ONE **2:** e718

Wu FH, Shen SC, Lee LY, Lee SH, Chan MT, Lin CS (2009) Tape-Arabidopsis sandwich: a simpler Arabidopsis protoplast isolation method. Plant Methods **5:** 16

Xue S, Hu H, Ries A, Merilo E, Kollist H, Schroeder JI (2011) Central functions of bicarbonate in S-type anion channel activation and OST1 protein kinase in CO_2 signal transduction in guard cell. EMBO J **30:** 1645–1658